

Evaluation of the GSO:Ce scintillator in the X-ray energy range from 40 to 140 kV for possible applications in medical X-ray imaging

D. Nikolopoulos^a, I. Valais^{a,b}, I. Kandarakis^{a,*}, D. Cavouras^a, D. Linardatos^a, I. Sianoudis^c, A. Louizi^d, N. Dimitropoulos^e, D. Vattis^c, A. Episkopakis^a, C. Nomicos^f, G. Panayiotakis^b

^aDepartment of Medical Instruments Technology, Technological Educational Institution of Athens, Agiou Spyridonos Street, Aigaleo, 12210 Athens, Greece

^bMedical Physics Department, University of Patras, Greece

^cDepartment of Physics, Chemistry and Materials Technology, Technological Educational Institution of Athens, 12210 Athens, Greece

^dMedical Physics Department, University of Athens, Greece

^eDepartment of Medical Imaging, Euromedica Medical Center, 2 Mesogeion Ave., Athens, Greece

^fDepartment of Electronics, Technological Educational Institution of Athens, 12210 Athens, Greece

Received 12 July 2005; received in revised form 6 December 2005; accepted 29 December 2005

Available online 24 January 2006

Abstract

The purpose of the present study was to evaluate, under X-ray medical imaging conditions, the X-ray luminescence efficiency (XLE) and the optical quantum gain (OQG) of the Gd₂SiO₅:Ce scintillator in single crystal form, suitable for tomographic applications. Intrinsic physical properties and light emission characteristics of the Gd₂SiO₅:Ce scintillator, were also studied. Both experimental and Monte Carlo techniques were used. Various X-ray tube voltages (40–140 kV), currently employed in X-ray imaging applications, were used. XLE was found to vary slowly with X-ray tube voltage from (0.021 ± 0.003) to (0.017 ± 0.003) . OQG varied from (317 ± 18) to (466 ± 23) light photons per incident X-ray. These values were adequately high for imaging applications using the particular energy range. Additionally, it was found by Monte Carlo simulations that for crystal thicknesses higher than 0.5 cm both XLE and OQG reached saturation levels, indicating that higher thickness crystals are of no practical use in X-ray medical imaging.

© 2006 Elsevier B.V. All rights reserved.

PACS: 78.60; 07.85; 78.65; 42.20

Keywords: Scintillators; X-ray imaging; Luminescence efficiency; Radiation detectors

1. Introduction

Most of the radiation detectors used in medical imaging, either in diagnostic radiology (X-ray radiography, fluoroscopy, mammography, computed tomography) or in nuclear medicine (gamma camera, positron emission tomography), are based on scintillator-optical detector combinations. In such combinations, scintillators are employed as single crystals, ceramic layers or powder screens. Scintillators are deposited on or brought in close contact to optical detectors, such as photodiode arrays,

photocathodes, charge coupled devices or radiographic films [1–3].

Among the various scintillators, particular interest has been paid on gadolinium oxyorthosilicate (Gd₂SiO₅ or GSO), often doped with cerium (Ce³⁺) ion activator (GSO:Ce). This material was firstly introduced by Takagi and Fukazawa [4]. GSO:Ce is of high density ($\rho = 6.71 \text{ g/cm}^3$) and high effective atomic number ($Z_{\text{Gd}} = 69$) providing high radiation absorption efficiency. Its light spectrum peaks at 440 and 490 nm while its refractive index is equal to 1.8. In addition, GSO:Ce exhibits a very fast response with a decay time of 60 ns. This is due to the Ce³⁺ ion activator energy level scheme, inducing a fast de-excitation via a $5d^1 \rightarrow 4f^1$ radiative transition [3,5]. The properties of high radiation detection

*Corresponding author. Tel.: +30210 5385 387/5385 375; fax: +30210 5910 975.

E-mail address: kandarakis@teiath.gr (I. Kandarakis).

and fast decay time, are very interesting for X-ray imaging detectors since: (i) the total amount of radiation energy absorbed within the scintillator's mass is crucial for the overall performance of detectors used in X-ray imaging, (ii) the patient dose burden may be reduced when high absorption detectors are used and (iii) the currently employed X-ray imaging scintillators (CsI, Gd₂O₂S, etc.) have slower decay time than GSO:Ce [6–9].

GSO:Ce has been previously studied under excitation with electrons, γ -rays [10], high energy (500 keV) X-rays [11], charged particles [12,13] and UV radiation [14]. Up to now, GSO:Ce has been used commercially only in positron emission imaging detectors [15]. To our knowledge, GSO:Ce has never been used either in conventional or in digital and tomographic X-ray imaging detectors both requiring relatively low energy X-rays (lower than 150 kV) [7,8]. In a recent study by our group [16], experimental data on the GSO:Ce scintillator were reported mainly concerning the experimental absolute efficiency and the spectral compatibility to optical sensors.

The purpose of the present study was to further investigate the efficiency of the GSO:Ce scintillator by evaluating light emission properties and intrinsic characteristics under X-ray diagnostic imaging irradiation conditions (40–140 kV X-rays). In particular, the X-ray luminescence efficiency (XLE), the optical quantum gain (OQG), and the intrinsic properties related to X-ray absorption, X-ray to light conversion, and light transmission properties of the GSO:Ce were studied, employing experimental and Monte Carlo techniques. This evaluation may be considered useful in investigating this material's suitability for use in fast response detectors, e.g., in X-ray computed tomography and in, recently introduced, X-ray computed tomography breast imaging [17,18], and may be of interest for possible applications to synchrotron radiation imaging [19].

2. Materials and methods

2.1. Theoretical aspects

The X-ray luminescence efficiency (η_L) is related to the scintillator's energy conversion properties and expresses the fraction of incident radiation energy converted into emitted light. XLE is defined as the ratio of the emitted light energy flux ($\dot{\Psi}_\lambda$) over the incident X-ray energy flux ($\dot{\Psi}_X$), according to formula (1) [20,21]

$$\eta_L = \frac{\dot{\Psi}_\lambda}{\dot{\Psi}_X} \quad (1)$$

where both $\dot{\Psi}_\lambda$ and $\dot{\Psi}_X$ are expressed in $\mu\text{W m}^{-2}$. XLE is suitable for evaluation of energy integrating detectors, mainly used in X-ray diagnostic radiology. These detectors produce an output signal directly proportional to the amount of total energy absorbed within the scintillator mass.

The detector optical quantum gain is a parameter expressing the scintillator's performance in terms of gain, i.e., the number of quanta produced at the scintillator's output per quantum at the scintillator's input. OQG has been defined [22] as the ratio of the emitted light photon flux ($\dot{\Phi}_\lambda$) over the incident X-ray photon flux ($\dot{\Phi}_X$):

$$G = \frac{\dot{\Phi}_\lambda}{\dot{\Phi}_X} \quad (2)$$

Both fluxes are expressed in number of photons per unit of area and time. OQG values are of the order of 10^2 – 10^3 . OQG is very often used in assessing imaging parameters of statistical nature, e.g., the mean value of the number of photons and the corresponding standard deviation, often taken into account for signal to noise ratio assessment [6,23]. OQG is also useful in evaluating photon-counting detectors, such as those used in nuclear medicine imaging.

XLE and OQG may be also expressed in terms of intrinsic physical properties of the scintillator as shown in Eqs. (3) and (4) [20,22]

$$\eta_L = \eta_Q \eta_C g_L \quad (3)$$

$$G = \eta_Q m_0 g_L \quad (4)$$

where η_Q is the X-ray quantum detection efficiency of the scintillator, expressing the fraction of incident X-rays detected, η_C is the intrinsic X-ray to light conversion efficiency, which is the fraction of absorbed X-ray energy converted into light energy in the scintillator [22], m_0 is the intrinsic quantum conversion gain, being equal to the mean number of optical photons produced within the scintillator per X-ray quantum detected and g_L is the light transmission efficiency or transparency of the scintillator expressing the fraction of m_0 transmitted through the scintillator, i.e., from the point of light photon creation to the emitting surface. It must be noted that the detection efficiency (η_Q) is affected by the re-emission and escape of K-fluorescence characteristic X-rays. K-characteristic photon re-emission follows a photoelectric absorption, which is the dominant X-ray detection mechanism within the energy range employed in X-ray imaging.

2.2. Experiments, calculations and Monte Carlo simulations

Experimental techniques and Monte Carlo calculations were applied for the determination of the XLE, OQG, X-ray quantum detection efficiency (η_Q), the light transmission efficiency (g_L) and the intrinsic X-ray to light conversion efficiency (η_C). Monte Carlo techniques were also applied in the investigation of the variation of XLE and OQG with crystal thickness.

Measurements were performed on a GSO:Ce crystal of $10\text{ mm} \times 10\text{ mm} \times 10\text{ mm}$ dimensions doped with 0.5% mole concentration of Ce^{+3} , supplied by Hitachi Chemical Co. Ltd [24].

2.2.1. Experimental determination of the X-ray luminescence efficiency

XLE was experimentally determined in accordance with Eq. (1) by performing measurements of the light energy flux ($\dot{\Psi}_\lambda$) and the X-ray energy flux ($\dot{\Psi}_X$). The GSO:Ce crystal was irradiated by X-rays in a Philips Optimus X-ray unit. The latter was equipped with a tungsten target anode and 2 mm of aluminum (Al) filter. The X-ray beam was additionally filtered by 20 mm of aluminium, used for the simulation of the beam's hardening by a human body. X-ray tube voltage ranged between 40 and 140 kV, which is an energy range employed in X-ray computed tomography and in the, recently introduced, X-ray breast computed tomography imaging [17]. All measurements were performed using constant tube current (63 mAs). Since both light flux and X-ray flux are directly proportional to this current, it was assumed that XLE, defined as the ratio of these two quantities, is not affected by tube current variations.

The light energy flux ($\dot{\Psi}_\lambda$) emitted at the rear crystal surface, was measured using an EMI 9798B photomultiplier with an extended sensitivity S-20 (E-S20) photocathode coupled to a Cary 401 vibrating reed electrometer. The experimental data were corrected by taking into account the following factors: (i) The spectral matching factor expressing the compatibility between the light emission spectrum of GSO:Ce and the spectral sensitivity of the photomultiplier's (E-S20) photocathode. (ii) The geometric light collection efficiency of the crystal-photomultiplier experimental arrangement, expressing the fraction of the emitted light impinging at the photocathode surface. To assess the spectral matching factor [16,22], the emitted light spectrum and the spectral sensitivity of the photomultiplier were determined. The emitted light spectrum ($S_\lambda(\lambda)$) was directly measured, during X-ray excitation of the scintillator, using an Ocean Optics (Ocean Optics Inc., S2000) optical grating monochromator. The spectral sensitivity of the photomultiplier was determined by measuring the response of the photomultiplier to a series of prototype light emitting diodes (LED, Kingbright Company) emitting at various wavelengths, ranging from violet to red colour. The geometric light collection efficiency was assessed by taking into account the distance between the rear surface of the crystal and the front surface of the photocathode, the corresponding areas and the angular distribution of the emitted light, which was assumed to be lambertian.

The X-ray energy flux ($\dot{\Psi}_X$) was determined from X-ray exposure data (\dot{X}) collected by a Radcal 2026C dosimeter and by using the conversion formula (5) [22,25]

$$\dot{\Psi}_X = \frac{\dot{X}}{(\bar{\mu}_{\text{en}}/\rho)_{\text{air}}} \left(\frac{W_A}{e} \right) \quad (5)$$

where $(\bar{\mu}_{\text{en}}/\rho)_{\text{air}}$ is the X-ray mass energy absorption coefficient of air, averaged over the X-ray spectrum, and (W_A/e) is the average energy per unit of charge required to

produce an electron-ion pair in air. The values of (W_A/e) and $(\bar{\mu}_{\text{en}}/\rho)_{\text{air}}$ were obtained from the literature [25,26].

2.2.2. Experimental determination of the optical quantum gain

The optical quantum gain was determined according Eq. (2) by calculating the photon fluxes $\dot{\Phi}_\lambda$ and $\dot{\Phi}_X$ from the experimentally determined energy fluxes $\dot{\Psi}_\lambda$ and $\dot{\Psi}_X$ by using Eqs. (6) and (7) [22]

$$\dot{\Phi}_\lambda = \frac{\dot{\Psi}_\lambda}{\bar{E}_\lambda} \quad (6)$$

$$\dot{\Phi}_X = \frac{\dot{\Psi}_X}{\bar{E}_X} \quad (7)$$

where \bar{E}_λ is the mean energy of light photons emitted by the scintillator and \bar{E}_X the mean energy of the incident X-ray photons. \bar{E}_λ and \bar{E}_X were calculated using the measured GSO:Ce light emission spectrum $S_\lambda(\lambda)$ and the incident X-ray spectrum $S_X(E)$, respectively, in Eqs. (8) and (9)

$$\bar{E}_\lambda = hc \left[\frac{\int S_\lambda(\lambda) \lambda d\lambda}{\int S_\lambda(\lambda) d\lambda} \right]^{-1} \quad (8)$$

$$\bar{E}_X = \frac{\int S_X(E) E dE}{\int S_X(E) dE} \quad (9)$$

where E is the energy of an X-ray photon. $S_X(E)$ was determined as described by Boone [8].

2.2.3. Experimental determination of the light transmission efficiency

The light transmission efficiency (g_L) was experimentally determined by irradiating the GSO:Ce crystal by UV and visible light by a Perkin-Elmer UV/Visible lambda 15 Spectrophotometer with range of emitted wavelengths ranging from 200 to 900 nm. A UV/Visible light lamp was positioned at 10 cm in front of the entrance surface of the GSO:Ce crystal. UV and visible light transmitted through the crystal and escaping the back surface of the crystal was detected and measured by the spectrophotometer. The light transmission efficiency was calculated as the ratio of the detected over the incident light intensity.

2.2.4. Monte Carlo determination of the X-ray quantum detection efficiency

The X-ray detection efficiency (η_Q) was estimated employing custom Monte Carlo techniques developed by our group. Monte Carlo codes were developed using the Microsoft FORTAN Developer PC platform. The codes were designed so as to be efficient for applications in the diagnostic medical imaging energy range. Photon transport modelling was based on the three processes governing photon interactions in that energy range i.e. coherent and incoherent scattering and photoelectric absorption. An iterative procedure was used; a photon of certain energy was generated and considered to hit the entrance surface of

the scintillator block of predefined dimensions under known direction angles. Using random numbers and cross-sectional data, the mean-free photon path, as well as the site and type of the subsequent photon interaction were determined. In the case of scatter and by employing a method proposed by Chan and Doi [27], based on the use of the form and scatter factors of the materials under study, the photon transport parameters were calculated, i.e. photon energy and direction angles after the interaction and energy transferred to the electrons of the medium. The cross section values of the GSO:Ce were calculated using the XCOM code, which was based on the tables of Hubbell and Seltzer [28]. The XCOM code was downloaded from the NIST reference database [29]. The form factors and the scatter factors of the GSO:Ce were calculated from those corresponding to the elements constituting the scintillator using specially designed codes. The factors for the elements were also downloaded from the NIST reference database. The iterative procedure was continued until the photon escaped from- or was absorbed within, the scintillator block. In the latter case, all energy of the photon was considered to be transferred to the medium except of a part, which was considered to refer to the generation of characteristic fluorescence radiation or Auger electrons. Selection between characteristic fluorescence radiation and Auger electrons was based on a random number generation routine. In the case of characteristic fluorescence radiation simulation, photons were modelled as independent K- or L-characteristic quanta initiating their history at the photoelectric interaction site. The transport of these characteristic photons was simulated similarly to the transport of the primary ones. The characteristic fluorescence photons were generated with azimuthally uniform distribution. In the case of Auger electron production simulation, the part of the energy referring to Auger electrons was considered to be completely transferred to the scintillator block at the site of interaction. Various Monte Carlo simulation runs were performed. In every run 10^7 photons were generated and traced. All photon track and energy histories were recorded for further analysis. To study crystal properties at various thicknesses, scintillator crystals were modelled as a series of scintillating blocks of various thicknesses. The blocks were of 1 cm^2 entrance area and of thicknesses ranging from 1 mm to 1 cm.

2.2.5. Evaluation of the intrinsic X-ray to light conversion efficiency

The intrinsic X-ray to light conversion efficiency (η_C) was determined according to Eq. (3), by taking into account the experimentally determined values of XLE and g_L and the Monte Carlo calculated values of η_Q for the $1 \times 1 \times 1\text{ cm}^3$ experimentally investigated GSO:Ce crystal.

2.2.6. Evaluation of the intrinsic quantum conversion gain

The intrinsic quantum conversion gain, m_0 in Eq. (4), was found using the experimentally determined values of OQG and g_L and the Monte Carlo calculated values of η_Q

again for the $1 \times 1 \times 1\text{ cm}^3$ experimentally investigated GSO:Ce crystal.

2.2.7. Variation of XLE and OQG as a function of scintillator thickness

To investigate the effect of varying crystal thickness on the XLE and the OQG and to obtain an estimation of the performance of GSO:Ce at photon energies lower than those available in our experimental conditions, Eqs. (3) and (4) were used to calculate XLE and OQG values at various crystal thickness (ranging from 0.1 to 1 cm) and at different monoenergetic incident photon energies (20, 80 and 140 keV). This was achieved by combining the experimentally determined value of g_L , the estimated mean value of η_C , together with the values of η_Q and m_0 , determined from the Monte Carlo runs at the aforementioned thickness. Monoenergetic photon energy values (20, 80 and 140 keV) were suitably selected as representative of the mean X-ray energies corresponding to tube voltages used in various applications such as X-ray mammography (25–30 kV), in synchrotron imaging and X-ray computed tomography (130–140 kV), as well as in γ -ray imaging with ^{99m}Tc (140 keV), respectively.

3. Results and discussion

Figs. 1 and 2 present the variation of XLE and OQG with X-ray tube voltage, respectively for the 1 mm thick GSO:Ce crystal. XLE was found to vary slowly from (0.021 ± 0.003) at 50 kV to (0.017 ± 0.003) at 140 kV, exhibiting a slight tendency to decrease at high X-ray energies. OQG was found to vary from (317 ± 18) at 50 kV to (466 ± 23) at 140 kV and the corresponding OQG curve showed a tendency to increase with X-ray tube voltage. The shape of the OQG curve is quite different from that of the XLE curve. Fig. 3 presents the experimental data, as displayed by the Perkin–Elmer Spectrophotometer, collected for the determination of the light transmission efficiency of the GSO:Ce crystal. The g_L value estimated from these was 91.4% at 440 nm and 92.1% at 490 nm, with an average of $(91.7 \pm 0.2)\%$ at the wavelengths of

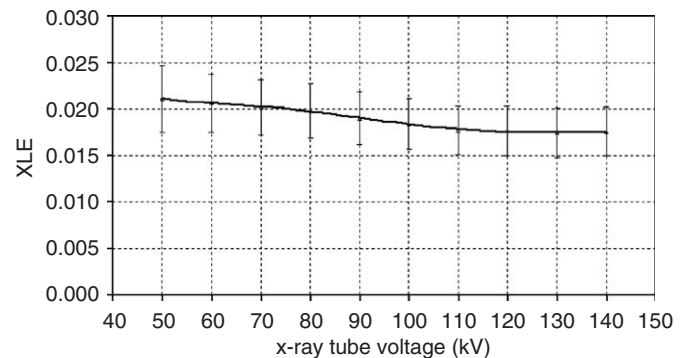


Fig. 1. XLE of the GSO:Ce scintillator as a function of the X-ray tube voltage. The solid line represents the best polynomial fit ($R^2 = 0.98$) to the measured data.

GSO:Ce emission (440–490 nm). Regarding the quantum detection efficiency of the GSO:Ce crystal, as determined by Monte Carlo simulation runs, it was found to be very high (above 90%) in the whole energy range. Table 1 presents detection efficiency data corresponding to 20 and 140 keV monoenergetic X-ray pencil beams, incident at the centre of the GSO:Ce crystal entrance area. In the same table, data derived by the MCNP 4c (Monte Carlo N-Particle) code are also shown for comparison purposes. As can be seen, the results are in close agreement with a maximum difference of 1.5%. The value for the intrinsic X-ray to light conversion efficiency evaluated from the above data was (0.020 ± 0.001) . Fig. 4 presents the variation of the

intrinsic quantum conversion gain m_0 as a function of X-ray tube voltage. m_0 increased linearly with X-ray tube voltage and it was found to vary between 310 and 540 in the energy range from 50 to 140 kV. Figs. 5 and 6 present data calculated out of the runs of the Monte Carlo simulation codes for the three selected energies, i.e., 20, 80 and 140 keV. These figures show the variation of the XLE and the OQG of GSO:Ce with thickness and were generated using the values of g_L and η_C already determined. For all selected energies, XLE was found to increase with thickness up to a certain crystal thickness. For the 20 and 80 keV simulated exposures this thickness was 0.2 cm, while for the 140 keV exposure, this was 0.6 cm. Thereafter, the XLE was constant with thickness. Non-significant differences between the XLE of the 20 keV and that of the 80 keV simulated exposures were observed. Above the thickness of 0.2 cm, OQG was constant for both 20 and 80 keV simulated exposures to within $\pm 1\%$. At 20 keV, OQG increased from 100 to 130 light photons per incident X-ray in the thickness range from 0.1 to 0.2 cm. At 80 keV, the corresponding values were 460 and 500 light photons per incident X-ray, respectively. At 140 keV, OQG ranged from 350 to 940 light photons per incident X-ray, for thicknesses from 0.1 to 0.5 cm.

The shape of the XLE curve (Fig. 1) may be explained in terms of three intrinsic properties of the GSO:Ce crystal: (i) the X-ray quantum detection efficiency, (ii) the intrinsic X-ray to light conversion efficiency and (iii) the light transmission efficiency. Regarding the X-ray quantum detection efficiency, this was found very high at the whole energy range; however, decreasing slightly with increasing X-ray tube voltage. This slight decrease affects the corresponding decrease of the XLE curve. Regarding the effect of the intrinsic X-ray to light conversion efficiency, this is not expected to depend on the incident X-ray energy and hence, only the absolute XLE values and the corresponding curve level are affected. Regarding GSO:Ce light transmission efficiency, it is of equally high values in the whole X-ray tube voltage range, due to the low importance of the light attenuation effects within the crystal (Fig. 3). Thus, it may be concluded that also only the level of the XLE curve is affected.

Similarly, the shape of OQG curve may be also explained in terms of three intrinsic properties of GSO:Ce crystal: (i) the intrinsic quantum conversion gain, (ii) the X-ray

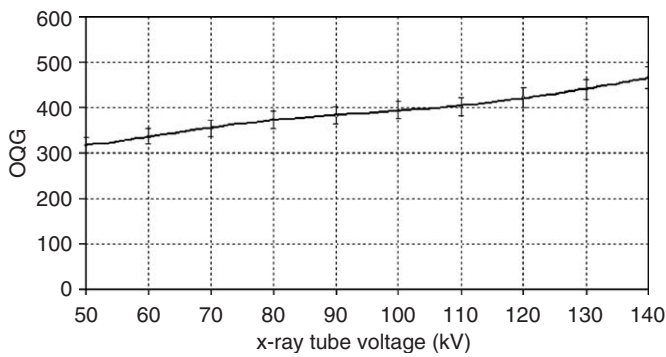


Fig. 2. Calculated OQG for the GSO:Ce scintillator as a function of the X-ray tube voltage. The solid line represents the best polynomial fit ($R^2 = 0.42$) to the measured data.

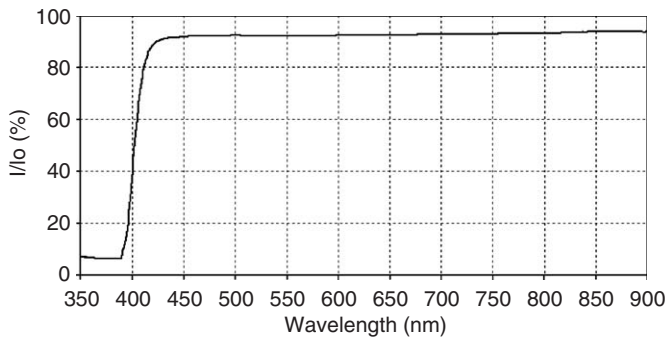


Fig. 3. Light transmission measurements performed with the UV/Visible Spectrometer. (I/I_o) represents the ratio of the transmitted over the incident light intensity.

Table 1

Detection efficiency of a $1 \times 1 \times 1 \text{ cm}^3$ GSO:Ce crystal for 20 and 140 keV photons incident at the centre of the entrance crystal area at a pencil beam geometry

| | 0.25 cm | | 0.50 cm | | 0.75 cm | | 1.00 cm | |
|---------|---------|----------|---------|----------|---------|----------|---------|----------|
| | MCNP | Our code | MCNP | Our code | MCNP | Our code | MCNP | Our code |
| 20 keV | 1 | 0.996 | 1 | 0.997 | 1 | 0.997 | 1 | 0.997 |
| 140 keV | 0.790 | 0.802 | 0.957 | 0.961 | 0.991 | 0.994 | 0.998 | 1 |

The efficiency was calculated by our Monte Carlo code at various crystal thickness. Data derived by the MCNP code for the same conditions are also given for comparison.

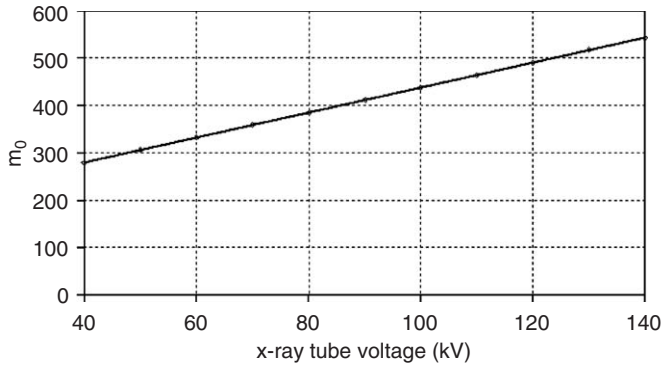


Fig. 4. Variation of the intrinsic quantum conversion gain with X-ray tube voltage.

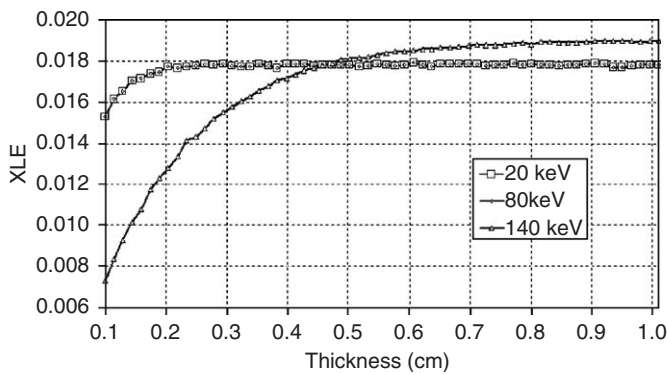


Fig. 5. Variation of XLE with crystal thickness at 20, 80 and 140 keV.

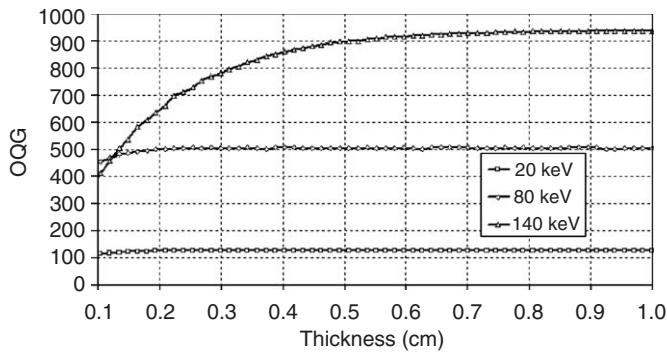


Fig. 6. Variation of OQG with crystal thickness at 20, 80 and 140 keV.

detection efficiency and (iii) the light transmission efficiency. The intrinsic quantum conversion gain increases linearly with X-ray tube voltage and therefore, it affects the corresponding variation of OQG. This may be explained by the fact that OQG expresses the number of optical photons per incident X-ray. As the X-ray tube voltage increases, the absorbed energy per X-ray photon absorbed increases accordingly. This absorbed energy is converted to energy of light photons. Since the light photons have always the same energy, their number is larger resulting in higher OQG values. On the other hand, the light

transmission efficiency affects only the level of OQG curve for similar reasons as explained earlier.

The results concerning the variation of XLE and OQG with thickness, show saturation of both these metrics at thick crystals. These results indicate that a 0.5 cm thick GSO:Ce crystal may be adequately efficient for use in most medical imaging applications including X-ray tomography, single γ -ray photon emission tomography, synchrotron radiation techniques, etc. [19].

To our knowledge, data on XLE and OQG have not been published for scintillators in single crystal form and in the energy range used in diagnostic radiology. However, to compare our results to tabulated data reported by van Eijk [3], we have calculated the number of emitted light photons per absorbed X-ray (light yield). The calculation was performed for an 1 cm thick GSO:Ce crystal irradiated by 140 keV monoenergetic X-rays, taking into account, that this crystal's quantum detection efficiency at 140 keV is 94.6%, as calculated from the Monte Carlo runs. Our result was 994 light photons per absorbed X-ray, which is approximately equal to the reported value [3] of 1000 light photons per absorbed X-ray. Moreover, our estimated value for the intrinsic X-ray to light conversion efficiency of (0.020 ± 0.001) is in agreement to the value of 0.025 reported by Blasse and Grabmaier [5].

Acknowledgments

This work was financially supported by the research program "EPEAEK Archimidis". The authors gratefully acknowledge Hitachi Chemical Co. for supplying the GSO:Ce crystal.

References

- [1] H.J. Besch, Nucl. Instr. and Meth. A 419 (1998) 201.
- [2] A. Del Guerra, M.G. Bisogni, C. Damiani, G. Di Domenico, R. Marchesini, G. Zabattini, Nucl. Instr. and Meth. A 442 (1–3) (2000) 18.
- [3] C.W.E. van Eijk, Nucl. Instr. and Meth. A 460 (2001) 1.
- [4] K. Takagi, T. Fukazawa, Appl. Phys. Lett. 42 (1983) 43.
- [5] G. Blasse, B.C. Grabmaier, Luminescent Mater., Springer, Berlin, Heidelberg, 1994.
- [6] J.A. Rowlands, Flat Panel Detectors for Digital Radiography, Handbook of Medical Imaging, Physics and Psychophysics, SPIE Press, Bellingham, 2000.
- [7] M.J. Yaffe, J.A. Rowlands, Phys. Med. Biol. 42 (1997) 1.
- [8] J.M. Boone, X-ray production, Interaction, and Detection in Diagnostic Imaging, in: J. Beutel, H.L. Kundel, R.L. Van Metter (Eds.), Handbook of Medical Imaging, Physics and Psychophysics, vol. 1, SPIE Press, Bellingham, 2000.
- [9] C.W.E. van Eijk, Phys. Med. Biol. 47 (2002) R85.
- [10] W. Mangesh, T.D. Taulbee, J.D. Valentine, B.D. Rooney, Nucl. Instr. and Meth. A 486 (2002) 448.
- [11] T. Kamae, Y. Fukazawa, N. Isobe, M. Kokubun, A. Kubota, S. Osone, T. Takahashi, N. Tsuchida, H. Ishibashi, Nucl. Instr. and Meth. A 490 (2002) 456.
- [12] T.A. DeVol, S.B. Chotoo, R.A. Fjeld, Nucl. Instr. and Meth. A 425 (1998) 228.
- [13] V. Avdeichikov, B. Jakobsson, V.A. Nikitin, V. Nomokonov, A. Wegner, Nucl. Instr. and Meth. A. 484 (2002) 251.

- [14] S. Shimizu, H. Ishibashi, A. Ejiri, S. Kubota, Nucl. Instr. and Meth. A. 486 (2002) 490.
- [15] J.S. Karp, S. Surti, M.E. Daube-Witherspoon, R. Freifelder, C.A. Cardi, L.E. Adam, K. Bilger, G. Muehllehner, J. Nucl. Med. 44 (2003) 1340.
- [16] I. Valais, I. Kandarakis, D. Nikolopoulos, I. Sianoudis, N. Dimitropoulos, D. Cavouras, C. Nomicos, G. Panayiotakis, IEEE Trans. Nucl. Sci. 52 (2005) 1830.
- [17] J.M. Boone, T.R. Nelson, K.K. Lindfors, J.A. Seibert, Radiology 221 (2001) 657.
- [18] B. Chen, R. Ning, Med. Phys 29 (2002) 755.
- [19] A. Gorin, K. Kuroda, I. Manuilov, A. Riazantsev, T. Ishikawa, H. Kamitsuo, M. Suzuki, H. Toyokawa, Nucl. Instr. and Meth. A 510 (2003) 76.
- [20] I. Kandarakis, D. Cavouras, G.S. Panayiotakis, C.D. Nomicos, Phys. Med. Biol. 42 (1997) 1351.
- [21] G.W. Ludwig, J. Electrochem. Soc. 118 (7) (1971) 1152.
- [22] I. Kandarakis, D. Cavouras, C.D. Nomicos, G.S. Panayiotakis, Nucl. Instr. and Meth. B 179 (2001) 215.
- [23] D. Cavouras, I. Kandarakis, E. Kanellopoulos, C.D. Nomicos, G.S. Panayiotakis, Appl. Rad. Isot. 51 (1999) 59.
- [24] Hitachi Chemical Co., Ltd., Internet site address: <http://www.hitachi-chem.co.jp/english/>.
- [25] J.R. Greening, Fundamentals of Radiation Dosimetry, Institute of Physics, London, 1985.
- [26] H.E. Johns, J.R. Cunningham, The Physics of Radiology, Springfield, IL, 1983.
- [27] H.P. Chan, K. Doi, Phys. Med. Biol. 28 (1983) 109.
- [28] J.H. Hubbell, S.M. Seltzer. Tables of X-ray mass attenuation coefficients and mass energy absorption coefficients 1 keV to 20 MeV for elements $Z = 1$ to 92 and 48 additional substances of dosimetric interest. US Department of commerce. NISTIR 5632, 1995
- [29] <ftp://physics.nist.gov/PhysRefData/>.